

Directional Goldstone waves in polariton condensates close to equilibrium

Dario Ballarini^{*,1}, Davide Caputo^{1,2}, Galbadrakh Dagvadorj^{3,4}, Richard Jiggins³,

Milena De Giorgi¹, Lorenzo Dominici¹, Kenneth West⁵, Loren N. Pfeiffer⁵,

Giuseppe Gigli^{1,2}, Marzena H. Szymańska³, and Daniele Sanvitto^{1,6}

¹*CNR NANOTEC—Institute of Nanotechnology, Via Monteroni, 73100 Lecce, Italy*

²*University of Salento, Via Arnesano, 73100 Lecce, Italy*

³*Department of Physics and Astronomy, University College London,
Gower Street, London WC1E 6BT, United Kingdom*

⁴*Department of Physics, University of Warwick, Coventry CV4 7AL, United Kingdom*

⁵*PRISM, Princeton Institute for the Science and Technology of Materials, Princeton University, Princeton, NJ 08540*

⁶*INFN, Sez. Lecce, 73100 Lecce, Italy*

Quantum fluids of light are realized in semiconductor microcavities by exciton-polaritons, solid-state quasi-particles with a light mass and sizeable interactions. Here, we use the microscopic analogue of oceanographic techniques to measure the excitation spectrum of a thermalised polariton condensate. Increasing the fluid density, we demonstrate the transition from a free-particle parabolic dispersion to a linear, sound-like Goldstone mode characteristic of superfluids at equilibrium. Notably, we show that excitations are created with a definite direction with respect to the condensate, analogous to how a sea breeze develops surface waves aligned with the wind. These results reveal the effect of asymmetric pumping on the collective excitations of a condensate. Furthermore, we measure the critical sound speed for polariton superfluids close to equilibrium.

Exciton-polaritons (hereafter polaritons) are bosons that condense in a driven-dissipative environment, where the steady state is achieved through a balance between gain and losses [1, 2]. In this two-dimensional system, the pump is usually a non-resonant laser that creates a large population of excitons (in a reservoir), which quickly relax into lower-energy polariton states. Dissipation mainly occurs through leakage from the cavity mirrors, requiring constant feeding from the pump and allowing the optical detection of the polariton field by photoluminescence (PL) measurements. Above a density threshold, macroscopic quantum degeneracy of polaritons has been demonstrated in a variety of materials and structures up to room temperature [3–6]. However, the fundamental dynamics of the collective excitations of polariton quantum fluids are often hidden by the microscopic details of the disorder environment and by the effect of pumping and dissipation.

The excitation spectrum of polariton condensates is modified by drive and decay with respect to the equilibrium case of cold atoms, and is diffusive rather than linear at small momenta [7, 8]. This is a general feature of driven-dissipative systems and prevents the Landau criterion from being fulfilled in non-resonantly pumped polariton condensates [9]. Recently, it has been suggested that the diffusive character of low-energy excitations can be strongly suppressed for long-lived polaritons (lifetimes longer than 100 ps) and further reduced if the polariton condensate is spatially separated from the exciton reservoir [10, 11].

Although in principle the excitation spectrum of polariton condensates is accessible through PL experiments, in practice its detection is seriously hindered by the low signal-to-noise ratio, the strong emission intensity from

the condensate itself and the relatively broad polariton resonances [12–15]. First indications of the existence of a soft Goldstone mode in time resolved experiments were obtained by the observation of a critical slowing down of the dynamics of an optical parametric amplifier [16, 17]. More recently, four-wave mixing experiments have highlighted the presence of the ghost branch, which appears with negative energies with respect to the condensate [14, 18–20]. However, so far any quantitative comparison has been challenging due to the short polariton lifetime and the small condensate size, limiting in energy and wavevector resolution a direct observation of the Goldstone spectrum.

In trapped atomic gases, Bragg scattering of two photons is used to detect collective excitations, allowing very accurate measurements of their energy and wavevector [21–23]. In the opposite limit of wave-particle duality, the Bogoliubov spectrum of photons in a hot atomic vapour has been recently measured by estimating the group velocity of transverse perturbations [24]. For quantum fluids of light, the excitation spectrum $S(k, \omega)$ can be directly measured by performing the Fourier transform (FT) of the intensity pattern in space and time, $S(k, \omega) = \text{FT} [|\psi(\mathbf{r}, t)|^2]$ [25]. A related technique is used to measure the dispersion of ocean waves by the FT of a time series of pictures taken from an aircraft: instead of measuring directly the water displacement, the light diffracted by the surface waves at different times is used to reconstruct the frequency-wavevector relation with high resolution [26].

In this Letter, we employ a high-quality semiconductor microcavity with a reduced density of defects and long polariton lifetime to form a condensate close to equilibrium and to measure the spectrum of its collective exci-

tations by interferometric measurements of temporal and spatial coherence. This represents the optical analogue of the oceanographic technique used to obtain the dispersion of surface waves (Supplemental Information). In our case, the spatio-temporal oscillations of the polariton condensate are obtained through the fluctuations of the first-order correlation function. Using this technique we observe, for the first time, the transition to a linearised dispersion with increasing particle density, showing the dominant phonon character of the Goldstone modes in a thermalised polariton superfluid. Interestingly, collective excitations form in the condensate with a preferential direction, much like surface waves in the ocean are oriented along the wind blowing in a specific direction. The origin of this peculiar effect in polariton condensates is due to the asymmetric pumping configuration which results in an asymmetrically populated Goldstone dispersion.

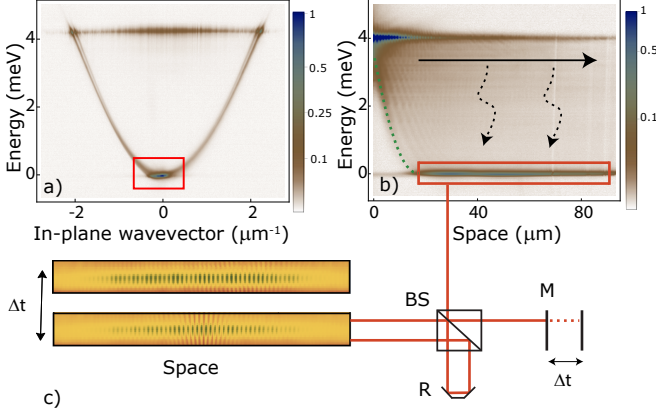


Figure 1: **a**, Momentum space PL showing the polariton dispersion. The energy offset is $E = 0$ at the bottom of the polariton dispersion, corresponding to 1.6 eV. **b**, Energy-resolved cross-section of real space PL. The pump is centred at $x=0$ and the Gaussian profile of the energy blueshift ($\Delta E \approx 4$ meV), due to the high density of excitons under the pump spot, is indicated by the green, dashed line. The expanding polariton flow is indicated by the black arrow at $E \approx 4$ meV, corresponding to the emission at $|k| = 2 \mu\text{m}^{-1}$ in **a**. The condensate is spatially separated from the pump and it is formed through phonon-mediated (dashed arrows) energy relaxation of the polaritons ballistically ejected from the pump position. The region marked by the red rectangle at the lowest energy corresponds to the emission at $k = 0$ in **a**. **c**, Interferogram for $\Delta t = 0$ and $\Delta t = 100$ ps obtained with a Michelson interferometer, where R is a corner mirror used to rotate the image around the autocorrelation point and a long delay line (M) has been included in the other arm.

The sample used in these experiments is a high quality factor ($Q > 10^5$) GaAs microcavity with a polariton lifetime of ≈ 100 ps and twelve 7-nm quantum wells placed at the positions of maximum field enhancement within the cavity [27–29]. The pump laser (tuned to the first minimum of the stop band, at $E = 1690$ meV, much higher than the polariton resonance) is focussed into a

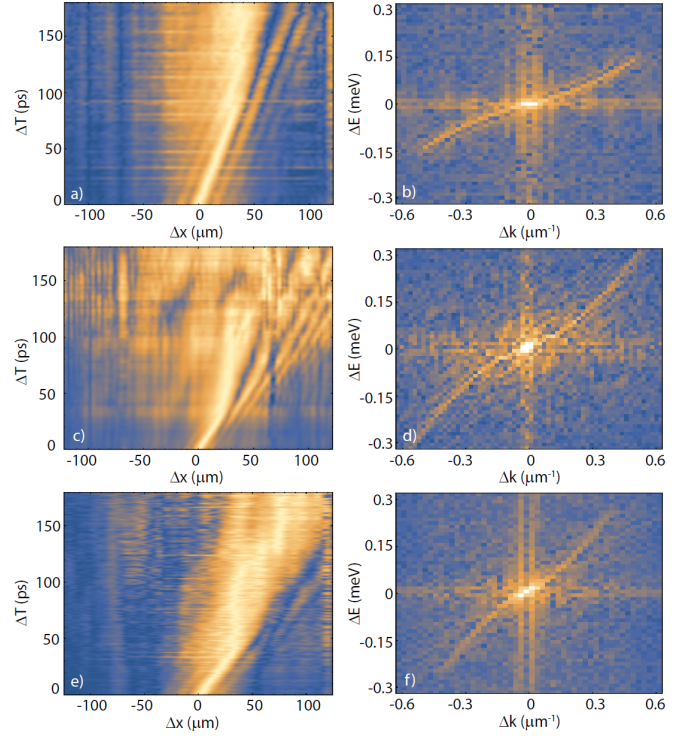


Figure 2: First order correlation function in space and time for increasing pumping powers (from top to bottom). $P = 0.9P_{th}$, $P = P_{th}$ and $P = 1.5P_{th}$ in **a**, **c**, **e**, respectively. **b**, **d**, **f**, The Fourier transforms of **a**, **c**, **e**, respectively.

Gaussian spot with diameter $\approx 10 \mu\text{m}$. After fast energy relaxation, a high density of excitons and polaritons is formed under the pump spot. As a consequence, an expanding cloud of polaritons ballistically propagate radially outwards from the injection point, while excitons, much heavier, are mainly localised within the pumping spot. In Fig. 1a-b, (showing momentum- and real-space cross sections, respectively) the k -delocalised emission at $E \approx 4$ meV comes from the high polariton density within the pump spot and the peaks at $|k| = 2 \mu\text{m}^{-1}$ correspond to polaritons radially expanding from the pump spot outward. Above a critical density, energy relaxation occurs efficiently in the expanding polariton cloud through stimulated scattering mediated by phonons, reducing the kinetic energy towards the bottom of the polariton dispersion and triggering the formation of a large polariton condensate with $k \approx 0$ all around the pumping spot [28, 30, 31]. The highest intensity peak (red rectangle) is measured at the bottom of the dispersion ($k = 0$) and is due to the emission coming from the extended condensate formed outside of the pump spot.

The signal coming from a region of the bottom condensate on the right side of the pump spot is sent to a Michelson interferometer with a corner reflector in one arm (R) and with a long delay line (M) in the other arm (Fig. 1c). An energy filter is applied to keep only the signal close (0.5 meV) to the bottom of the disper-

sion and avoid the contribution of higher-energy polaritons. The corner reflector is used to obtain the symmetric image around the central point (autocorrelation point), while the long delay line is used to measure the spatial correlations at different times. Selecting only the direction passing through the center of the image, the one dimensional interferogram is recorded for increasing delays to obtain, from the fringe visibility, the two-dimensional spatio-temporal correlation map $g^{(1)}(\Delta x, \Delta t)$. The condensate density can be controlled by externally tuning the intensity of the exciting laser and, in the left column of Fig. 2, $g^{(1)}(\Delta x, \Delta t)$ is shown for increasing polariton density from top to bottom. In the right column of Fig. 2, the two-dimensional Fourier transforms of $g^{(1)}(\Delta x, \Delta t)$ directly show the momentum-energy relations with increasing densities from top to bottom.

For a weakly-interacting many-boson system without drive and dissipation, the role of interactions can be addressed in the Bogoliubov approximation by introducing new quasi-particles, defined as a superposition of condensed particles, corresponding to forward and backward propagating waves [32]. The associated Bogoliubov dispersion has a positive and a negative branch of the form:

$$\hbar\omega_{bog}(k) = \pm \sqrt{\frac{\hbar^2 k^2}{2m} \left(\frac{\hbar^2 k^2}{2m} + 2\mu \right)} \quad (1)$$

where m is the particle mass, μ the self-interaction energy ($\mu = g|\psi|^2$ with g the particle-particle interaction strength and ψ the condensate wavefunction) and $k = \frac{p}{\hbar}$ the wavevector of the matter wave. The effect of the out-of-equilibrium configuration, with pumping and decay, is instead reflected in the following spectrum of elementary excitations

$$\omega_{ee}(k) = -i\Gamma/2 \pm \sqrt{\omega_{bog}^2 - \frac{\Gamma^2}{4}} \quad (2)$$

by the term Γ , which is a combination of pumping and dissipation rates [8, 9].

Experimental data are compared in Fig. 3 with the dispersion relation of Eq. 2 and with the single-particle dispersion $\frac{\hbar^2 k^2}{2m}$. The single-particle parabolic dispersion is measured from the momentum space PL well below the threshold power for condensation (Fig. 3a). To take into account the small, but still measurable, velocity of the condensate that tilts the excitation spectrum with respect to the reference frame, the Doppler term $\omega_{dop} = (k - k_c)v_c$ is added to Eq. 2. Moreover, to center the dispersion at the energy and wavevector of the condensate, the angular frequency $\omega_{offset} = v_c k_c$ is used, giving a total frequency term of $\omega_{tot} = \omega_{dop} + \omega_{ee} + \omega_{offset}$. Approaching the threshold (Fig. 3b), the measured excitation spectrum (points are obtained from the positions of the maximum intensity in the data shown in the right column of Fig. 2) cannot be distinguished from the bare dispersion (dashed line). Linearisation can instead be seen

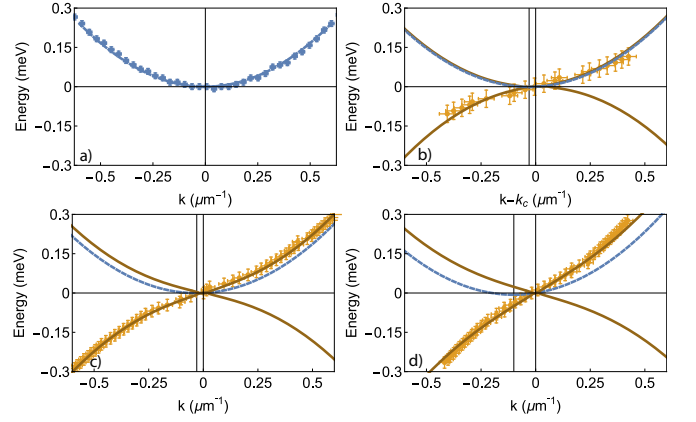


Figure 3: **a**, Parabolic dispersion extracted from PL at densities well below the condensation threshold d_{th} . **b**, **c**, **d**, Excitation spectrum for increasing pumping powers corresponding to $P = 0.9P_{th}$, $P = P_{th}$ and $P = 1.5P_{th}$ as extracted from the positions of the maxima in Fig. 2b,d,f, respectively. Best-fit parameters to Eq. 2 are $\mu = 0.005$ meV, $\mu = 0.04$ meV and $\mu = 0.1$ meV in **b**, **c**, **d**, respectively. The condensate wavevector is $k_c = 0.03 \mu\text{m}^{-1}$, $k_c = 0.03 \mu\text{m}^{-1}$ and $k_c = 0.1 \mu\text{m}^{-1}$ in **b**, **c**, **d**, respectively. The dashed-blue lines are the parabolic dispersion relations with the energy and momentum offsets given by μ and k_c as obtained from the fit of Eq. 2 to the data in each panel. The mass is extracted from the parabolic fitting of the data in **a**. $\Gamma = 0.005 \text{ ps}^{-1}$ is used in **b**, **c**, **d**.

in Fig. 3c and more clearly in Fig 3d. Bogoliubov quasi-particles behave as phonons ($\omega = c_s k$, with $c_s = \sqrt{\mu/m}$ the speed of sound) at small momentum $p \ll mc$ and as $\frac{\hbar^2 k^2}{2m} + 2\mu$, i.e. the single-particle dispersion with an additional frequency shift due to interactions, in the opposite limit of large momentum. From Fig. 3c to Fig. 3d, the sound speed extracted from the fitting curves increases from $0.35 \mu\text{m}/\text{ps}$ to $0.55 \mu\text{m}/\text{ps}$ and the healing length decreases from $\xi = 4 \mu\text{m}$ to $\xi = 2.5 \mu\text{m}$, giving cutoff wavevectors of $\frac{1}{\xi} \approx 0.24 \mu\text{m}^{-1}$ and $\frac{1}{\xi} \approx 0.38 \mu\text{m}^{-1}$, respectively. The fluid velocity also increases, from $v_f = 0.04 \mu\text{m}/\text{ps}$ in Fig 3c to $v_f = 0.13 \mu\text{m}/\text{ps}$ Fig 3d.

In Fig. 4, the points of Fig. 3d close to the condensate energy (energy resolution is given by $\delta E = \hbar \frac{2\pi}{T} = 0.02$ meV, with $T \approx 200$ ps the total time delay in the interferometric measurements) and wavevector are shown zoomed in. The sound dispersion $\omega = ck$ follows the experimental data for $k < 0.3 \mu\text{m}^{-1}$, while for larger wavevectors the excitation spectrum tends to recover the parabolic dispersion (dashed-gray line). At all densities, $\Gamma < 0.005 \text{ ps}^{-1}$, that is, the diffusive part of the excitation spectrum, where $\text{Re}[\omega_{ee}(k)] = 0$ (flat dispersion), is limited to only very small wavevectors $k < 0.007 \mu\text{m}^{-1}$, i.e. much smaller than the momentum resolution of the measurements ($\delta k = \frac{2\pi}{L}$, with $L \approx 100 \mu\text{m}$ the lateral size of the condensate). This means that the diffusive character of the excitation spectrum emerges only for distances

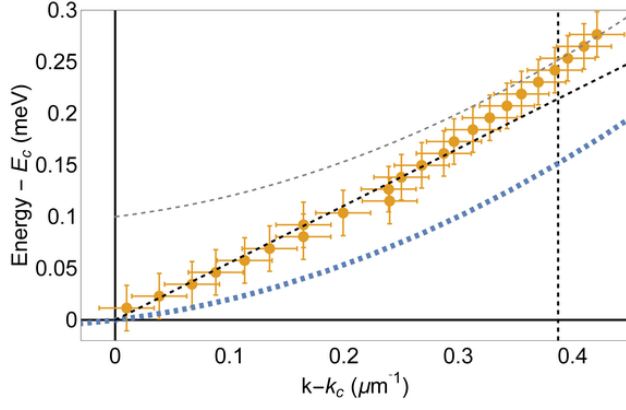


Figure 4: Experimental data of the excitation spectrum from Fig. 3d, zoomed in close to the condensate energy and momentum. The diagonal dashed-black line is the sound dispersion obtained from the same fitting parameters as used in Fig. 3d. Parabolic dispersion relations associated with the condensate energy and the high-momentum part of the spectrum are reported for clarity using dashed blue and grey lines, respectively. The vertical dashed line is the cutoff wavevector $\frac{1}{\xi}$ above which the dispersion is almost parabolic.

larger than the condensate itself.

As can be seen in Fig. 2 and Fig. 3, only one branch of the collective excitations, corresponding to forward propagating positive frequencies (and negative backward frequencies), is detected in the experiments. It is interesting to note that a finite condensate velocity only tilts the excitation spectrum in momentum space, and leaves the dispersion population symmetric. Our observations are instead very similar to measurements obtained for surface gravity waves in the presence of wind, for which only one branch can be observed (see SI). In our case, the directional driving force is ascribed to the asymmetric pumping configuration, where we consider only a portion of the condensate placed on the right-hand side of the pumping laser. The quantum and thermal fluctuations which populate the collective excitations of the condensate develop within the pump spot region where the exciton reservoir is localised and are mostly directed radially outwards, resulting in a negligible “up-wind” contribution to the excitation spectrum in our measurements.

To understand the physical origin of these observations, a numerical analysis based on the driven-dissipative Gross-Pitaevskii equation (GPE) for the polariton field ψ was performed with the same microscopic parameters. Specifically, the GPE is given by

$$i\hbar \frac{\partial \psi(\mathbf{r}, t)}{\partial t} = \left[-\frac{\hbar^2 \nabla^2}{2m} + i\frac{\hbar}{2} \left(\frac{\gamma(\mathbf{r})}{1 + \frac{|\psi(\mathbf{r}, t)|^2}{n_s}} - \kappa \right) + g|\psi(\mathbf{r}, t)|^2 + V(\mathbf{r}) \right] \psi(\mathbf{r}, t) \quad (3)$$

where $m \approx 3.8 \cdot 10^{-5} m_e$ is the polariton effective

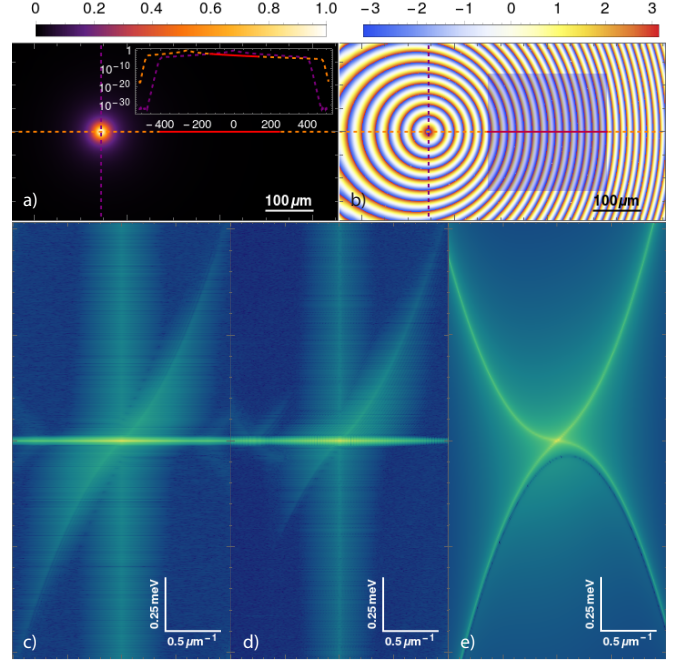


Figure 5: Numerical and analytical calculations of the spectrum and PL. **a**, Density profile of the condensate under the conditions of Fig. 1 with the pump placed on the left side of the measured region (solid red line in the horizontal profile). The main plot is on a linear scale and the inset a logarithmic one, showing the asymmetric polariton density of the condensate. **b**, Phase of the condensate in 2D space. The region under measurement is shown by the semitransparent rectangle. **c**, **d**, Excitation spectrum numerically obtained from the FT of $g^{(1)}(\Delta\mathbf{r}, \Delta t)$, i.e. following the same procedure as in the experiments, and of $|\psi(\mathbf{r}, t)|^2$, respectively. In the latter case the ghost branch is weakly populated, but still visible. **e**, PL from analytical calculations in the Bogoliubov approximation under uniform pumping. Note that in this case both branches are populated.

mass, $\gamma(\mathbf{r})$ is the Gaussian pump, $\kappa \approx 1/200 \text{ ps}^{-1}$ is the effective decay rate, and $g=0.004 \text{ meV } \mu\text{m}^2$ and $n_s=1000 \mu\text{m}^{-2}$ are the effective polariton-polariton interaction strength and the saturation density, respectively. In the spirit of truncated Wigner methods, we include thermal fluctuations by adding white noise as an initial condition and averaging over different realisations.

In Fig. 5, the asymmetric experimental configuration is replicated by appropriate numerical simulations. The wedge potential, given by

$$V(\mathbf{r}) = \frac{V_0}{L_0}(L - x)$$

where $V_0 = 0.1 \text{ meV}$ and $L_0 = 400.0 \mu\text{m}$, is used in the simulations shown in Fig. 5 to fully reproduce the experimental conditions but it is inessential to the physics observed here, as explicitly demonstrated in the SI. The pump is located at the bright spot where the dashed lines cross in Fig. 5a, while we measure the condensate on the

right-hand side of the pump (see also Fig. 5b, showing the phase of the condensate in 2D space with the region under consideration marked by a semitransparent rectangle). In the inset of Fig. 5a, we plot the polariton density along the horizontal and vertical cross sections passing through the pump, with a decreasing polariton density going from left to right in the region under consideration (indicated by the solid, red line). In Fig. 5c, we present the excitation spectrum obtained following the same procedure as for the experimental data, and showing that only one Bogoliubov branch is occupied, as in experiment. Note that the ghost branch appears populated in this case as a result of applying the Fourier transform to $g^{(1)}(\Delta\mathbf{r}, \Delta t)$, which is symmetric with respect to frequency. The true population of the ghost branch is shown in Fig. 5d, where the FT is applied to $|\psi(\mathbf{r}, t)|^2$ and the ghost branch appears much less populated than in Fig. 5c (but still visible). However, Fig. 5d also shows the experimentally observed directionality of excitations, which is therefore independent on the technique used in the experiments. In Fig. 5e, we show the PL obtained analytically in the Bogoliubov approximation for homogeneous (spatially uniform) pumping. The other parameters are the same as those in the inhomogeneously pumped simulations, including the same finite velocity of the condensate, but nonetheless the directionality of the excitations is lost.

In conclusion, we have shown that the collective excitations typical of equilibrium BEC survive in a driven-dissipative environment, demonstrating the phonon-like character of a Goldstone mode. To obtain the frequency-wavevector relation of the collective excitations of the condensate, we have measured the fluctuations of the correlation function in space and time, in analogy to oceanographic techniques measuring the dispersion of surface waves. Moreover, we have investigated the origin of the asymmetry in the population of the excitation spectrum, finding that the off-axis pumping configuration is responsible for the directionality of the Goldstone waves as it leads to a breeze of quantum fluctuations blowing on the condensate. These results show that long-lived polaritons manifest universal features typical of interacting bosons at equilibrium and open the door to the optical investigation and control of the collective excitations in open-dissipative condensates by engineering the reservoir topology.

The authors are grateful to I. Carusotto and I. Amelio for fruitful discussions and to P. Cazzato for technical support. This work has been funded by the POLAFLOW ERC Starting Grant and the ERC project ElecOpteR grant number 780757. M.H.S. gratefully acknowledges financial support from EPSRC (Grants no. EP/R04399X/1 and no. EP/K003623/2). The work at Princeton University was funded by the Gordon and Betty Moore Foundation through the EPIQS initiative Grant GBMF4420, and by the National Science Founda-

tion MRSEC Grant DMR 1420541.

-
- [1] A. Imamoglu, R. J. Ram, S. Pau, and Y. Yamamoto, *Phys. Rev. A* **53**, 4250 (1996).
 - [2] I. Carusotto and C. Ciuti, *Rev. Mod. Phys.* **85**, 299 (2013).
 - [3] J. Kasprzak, M. Richard, S. Kundermann, A. Baas, P. Jeambrun, J. M. J. Keeling, F. M. Marchetti, M. H. Szymańska, R. André, J. L. Staehli, et al., *Nature (London)* **443**, 409 (2006).
 - [4] R. Balili, V. Hartwell, D. Snoke, L. Pfeiffer, and K. West, *Science* **316**, 1007 (2007).
 - [5] K. S. Daskalakis, S. A. Maier, and S. Kéna-Cohen, *Phys. Rev. Lett.* **115**, 035301 (2015).
 - [6] G. Lerario, A. Fieramosca, F. Barachati, D. Ballarini, K. S. Daskalakis, L. Dominici, M. De Giorgi, S. A. Maier, G. Gigli, S. Kéna-Cohen, et al., *Nature Physics* **13**, 837 (2017).
 - [7] J. Keeling, P. R. Eastham, M. H. Szymanska, and P. B. Littlewood, *Phys. Rev. Lett.* **93**, 226403 (2004).
 - [8] M. H. Szymańska, J. Keeling, and P. B. Littlewood, *Phys. Rev. Lett.* **96**, 230602 (2006).
 - [9] M. Wouters and I. Carusotto, *Phys. Rev. Lett.* **99**, 140402 (2007).
 - [10] Y. Sun, P. Wen, Y. Yoon, G. Liu, M. Steger, L. N. Pfeiffer, K. West, D. W. Snoke, and K. A. Nelson, *Phys. Rev. Lett.* **118**, 016602 (2017).
 - [11] D. Caputo, D. Ballarini, G. Dagvadorj, C. Sanchez Munoz, M. De Giorgi, L. Dominici, K. West, L. Pfeiffer, G. Gigli, F. Laussy, et al., *Nature Materials* **17**, 145 (2018).
 - [12] S. Utsunomiya, L. Tian, G. Roumpos, C. W. Lai, N. Kumada, T. Fujisawa, M. Kuwata-Gonokami, A. Löffler, S. Höfling, A. Forchel, et al., *Nature Physics* **4**, 700 (2008).
 - [13] M. Pieczarka, M. Syperek, L. Dusanowski, J. Misiewicz, F. Langer, A. Forchel, M. Kamp, C. Schneider, S. Höfling, A. Kavokin, et al., *Phys. Rev. Lett.* **115**, 186401 (2015).
 - [14] T. Byrnes, T. Horikiri, N. Ishida, M. Fraser, and Y. Yamamoto, *Phys. Rev. B* **85**, 075130 (2012).
 - [15] M. Nakayama and M. Ueda, *Phys. Rev. B* **95**, 125315 (2017).
 - [16] M. Wouters and I. Carusotto, *Phys. Rev. A* **76**, 043807 (2007).
 - [17] D. Ballarini, D. Sanvitto, A. Amo, L. Viña, M. Wouters, I. Carusotto, A. Lemaitre, and J. Bloch, *Phys. Rev. Lett.* **102**, 056402 (2009).
 - [18] M. Wouters and I. Carusotto, *Phys. Rev. B* **79**, 125311 (2009).
 - [19] V. Kohnle, Y. Léger, M. Wouters, M. Richard, M. T. Portella-Oberli, and B. Deveaud-Plédran, *Phys. Rev. Lett.* **106**, 255302 (2011).
 - [20] V. Kohnle, Y. Léger, M. Wouters, M. Richard, M. T. Portella-Oberli, and B. Deveaud, *Phys. Rev. B* **86**, 064508 (2012).
 - [21] M. H. Anderson, J. R. Ensher, M. R. Matthews, C. E. Wieman, and E. A. Cornell, *Science* **269**, 198 (1995).
 - [22] D. S. Jin, J. R. Ensher, M. R. Matthews, C. E. Wieman, and E. A. Cornell, *Phys. Rev. Lett.* **77**, 420 (1996).

- [23] J. Steinhauer, R. Ozeri, N. Katz, and N. Davidson, *Phys. Rev. Lett.* **88**, 120407 (2002).
- [24] Q. Fontaine, T. Bienaimé, S. Pigeon, E. Giacobino, A. Bramati, and Q. Glorieux, *Phys. Rev. Lett.* **121**, 183604 (2018).
- [25] D. Vocke, T. Roger, F. Marino, E. M. Wright, I. Carusotto, M. Clerici, and D. Faccio, *Optica* **2**, 484 (2015).
- [26] J. P. Dugan, G. J. Fetzer, J. Bowden, G. J. Farruggia, J. Z. Williams, C. C. Piotrowski, K. Vierra, D. Campion, and D. N. Sitter, *Journal of Atmospheric and Oceanic Technology* **18**, 1267 (2001).
- [27] B. Nelsen, G. Liu, M. Steger, D. W. Snoke, R. Balili, K. West, and L. Pfeiffer, *Phys. Rev. X* **3**, 041015 (2013).
- [28] D. Ballarini, D. Caputo, C. S. Muñoz, M. De Giorgi, L. Dominici, M. H. Szymańska, K. West, L. N. Pfeiffer, G. Gigli, F. P. Laussy, et al., *Phys. Rev. Lett.* **118**, 215301 (2017).
- [29] E. Estrecho, T. Gao, N. Bobrovska, M. D. Fraser, M. Steger, L. Pfeiffer, K. West, T. C. H. Liew, M. Matuszewski, D. W. Snoke, et al., *Nature Communications* **9**, 2944 (2018).
- [30] T. D. Doan, H. T. Cao, D. B. Tran Thoai, and H. Haug, *Phys. Rev. B* **72**, 085301 (2005).
- [31] M. Wouters, T. C. H. Liew, and V. Savona, *Phys. Rev. B* **82**, 245315 (2010).
- [32] N. N. Bogolyubov, *J. Phys.(USSR)* **11**, 23 (1947), [*Izv. Akad. Nauk Ser. Fiz.*11,77(1947)].